Naval Research Laboratory
Washington, DC 20375-5320

NRL/8220/MR—2022/3

A Discontinuous Galerkin Method for Resistive Magnetohydrodynamics Using NRL's JENRE® Code

CHRISTIAN L. BACHMAN

Design and Verification Branch
Spacecraft Engineering Division

ANDREW D. KERCHER

Laboratories for Computational Physics and Fluid Dynamics
Materials Science and Component Technology Directorate

November 14, 2022

REPORT DOCUMENTATION PAGE

Form Approved
OMB No. 0704-0188

1. REPORT DATE *(DD-MM-YYYY)*	2. REPORT TYPE	3. DATES COVERED *(From - To)*
14-11-2022	NRL Memorandum Report	04-26-2020 – 04-25-2022

4. TITLE AND SUBTITLE

A Discontinuous Galerkin Method for Resistive Magnetohydrodynamics using NRL's JENRE® Code

5a. CONTRACT NUMBER

5b. GRANT NUMBER

5c. PROGRAM ELEMENT NUMBER
NISE

6. AUTHOR(S)

Christian L. Bachman and Andrew D. Kercher

5d. PROJECT NUMBER

5e. TASK NUMBER

5f. WORK UNIT NUMBER
N2W6

7. PERFORMING ORGANIZATION NAME(S) AND ADDRESS(ES)

Naval Research Laboratory
4555 Overlook Avenue, SW
Washington, DC 20375-5320

8. PERFORMING ORGANIZATION REPORT NUMBER

NRL/8220/MR--2022/3

9. SPONSORING / MONITORING AGENCY NAME(S) AND ADDRESS(ES)

Naval Research Laboratory
4555 Overlook Avenue, SW
Washington, DC 20375-5320

10. SPONSOR / MONITOR'S ACRONYM(S)
NRL-NISE

11. SPONSOR / MONITOR'S REPORT NUMBER(S)

12. DISTRIBUTION / AVAILABILITY STATEMENT

DISTRIBUTION STATEMENT A: Approved for public release; distribution is unlimited.

13. SUPPLEMENTARY NOTES
Karles Fellowship

14. ABSTRACT

We outline progress made towards the development of a computational model coupling electromagnetic effects with fluid dynamics for use in the study of ionized flows around hypersonic vehicles. The reported progress is on the implementation and validation of a resistive magnetohydrodynamics (MHD) solver using NRL's JENRE® Multiphysics Framework. This extends the existing groundwork for the development and use of more detailed and realistic modeling capabilities. We outline the numerical methods, implementation, and successful validation of the resistive MHD model using the unstructured computational mesh framework of the JENRE® code, which is novel in the field of MHD and will play a critical role in modeling realistic hypersonic vehicle geometries in the future.

15. SUBJECT TERMS

16. SECURITY CLASSIFICATION OF:			17. LIMITATION OF ABSTRACT	18. NUMBER OF PAGES	19a. NAME OF RESPONSIBLE PERSON
a. REPORT	b. ABSTRACT	c. THIS PAGE			Christian Bachman
U	U	U	U	28	19b. TELEPHONE NUMBER *(include area code)* (202) 767-8573

Standard Form 298 (Rev. 8-98)
Prescribed by ANSI Std. Z39.18

This page intentionally left blank.

CONTENTS

FIGURES

EXECUTIVE SUMMARY

We outline progress made towards the development of a computational model coupling electromagnetic effects with fluid dynamics for use in the study of ionized flows around hypersonic vehicles. The reported progress is on the implementation and validation of a resistive magnetohydrodynamics (MHD) solver using NRL's JENRE® Multiphysics Framework. This extends the existing groundwork for the development and use of more detailed and realistic modeling capabilities. We outline the numerical methods, implementation, and successful validation of the resistive MHD model using the unstructured computational mesh framework of the JENRE® code, which is novel in the field of MHD and will play a critical role in modeling realistic hypersonic vehicle geometries in the future.

This page intentionally left blank

A DISCONTINUOUS GALERKIN METHOD FOR RESISTIVE MAGNETOHYDRODYNAMICS USING NRL'S JENRE® CODE

1. INTRODUCTION

Hypersonic travel in Earth's atmosphere is often characterized by the presence of a partially ionized flow forming a plasma sheath around the vehicle. Hypersonic boost-glide and reentry vehicles can have flight Mach numbers ranging anywhere from 5 to 25, corresponding to highly varying plasma dynamics and characteristics, such as electron density, temperature, and ionization fraction. These plasma parameters play an important role in leading-edge heat flux, radio communication blackout, and increased radar cross-section [1–3]. Given the electromagnetic nature of these adverse effects, applied magnetic or electric fields can have a significant impact on mitigating them. This has become a promising area of research in the hypersonics community.

The historical difficulties in achieving hypersonic flight enthalpies in experimental facilities has made the study of relevant plasma chemistry equally as elusive and, although being pursued more in recent years [4], available flight test data is also limited and often dated [5]. For these reasons, numerical modeling remains the best method for studying plasmas within hypersonic flows and their interaction with electromagnetic fields. This motivates the implementation of an electromagnetic solver coupled with the fluid dynamics equations in the form of magnetohydrodynamics (MHD). We aim to do this by extension of NRL's existing fluid dynamic code, the JENRE® Multiphysics Framework.

The computational modeling of magnetized plasma as a continuum fluid through MHD has been studied for many years, primarly in an astrophysical context [6], in which the plasma is extremely hot, highly or fully ionized, and the magnetic field convects with the motion of the fluid. This is represented by ideal MHD, the implementation of which was the subject of a previous work [7]. The present work extends the existing model to include diffusive phenonena, namely the resistive diffusion of a magnetic field in an electrically conducting fluid. The added complexity over ideal MHD, and the dramatic expansion of relevant regimes that can be modeled, makes resistive MHD the natural step in progressing towards a more accurate and capable MHD solver for use in hypersonics.

In this paper we outline the implementation of a resistive MHD solver using the JENRE® code. The set of equations are presented as a coupling of the Navier-Stokes equations with Maxwell's equations for electromagnetism. We define the discontinuous Galerkin (DG) formulation and discretization of the equations, with reference to the key aspects of the prior ideal MHD development, and highlight the new aspects of the present model. The results from a series of benchmarks are presented then to validate our implementation. Lastly, we discuss the next steps that should be taken in order to achieve the ultimate goal of developing a numerical model that fully couples electromagnetism with fluid dynamics to model ionized flows in hypersonic regimes. The reader is encouraged to consider this, together with the previous work on the ideal MHD solver for a more complete picture of MHD development up to this point with the JENRE® code.

Manuscript approved October 12, 2022.

2. RESISTIVE MAGNETOHYDRODYNAMICS EQUATIONS

2.1 General derivation

To derive the resistive MHD equations we start with the compressible Navier-Stokes equations for a viscous, inert fluid and Maxwell's equations for electromagnetism. The two are linked through source terms representing the interaction of an electrically conducting fluid with electromagnetic fields.

$$\frac{\partial \rho}{\partial t} + \nabla \cdot (\rho \boldsymbol{v}) = 0 \tag{1}$$

$$\frac{\partial (\rho \boldsymbol{v})}{\partial t} + \nabla \cdot (\rho \boldsymbol{v}\boldsymbol{v} + P\boldsymbol{I} - \boldsymbol{\tau}) = \boldsymbol{J} \times \boldsymbol{B} \tag{2}$$

$$\frac{\partial \left(\rho \left(E + \frac{v^2}{2}\right)\right)}{\partial t} + \nabla \cdot \left(\left(\rho \left(E + \frac{v^2}{2}\right) + P\right)\boldsymbol{v} - \boldsymbol{\tau} \cdot \boldsymbol{v} - \kappa \nabla T\right) = \boldsymbol{E} \cdot \boldsymbol{J} \tag{3}$$

$$\nabla \cdot \boldsymbol{E} = \frac{\rho_c}{\epsilon_0} \tag{4}$$

$$\nabla \cdot \boldsymbol{B} = 0 \tag{5}$$

$$\nabla \times \boldsymbol{E} = -\frac{\partial \boldsymbol{B}}{\partial t} \tag{6}$$

$$\nabla \times \boldsymbol{B} = \mu_0 \left(\boldsymbol{J} + \epsilon_0 \frac{\partial \boldsymbol{E}}{\partial t}\right) \tag{7}$$

The viscous effects are included through the viscous stress tensor,

$$\boldsymbol{\tau} = \mu((\nabla \boldsymbol{v})^{\mathrm{T}} + \nabla \boldsymbol{v} - \frac{2}{3}\nabla \cdot \boldsymbol{v}\boldsymbol{I}), \tag{8}$$

where μ is the dynamic viscosity, and thermal conduction is included in the energy equation through the thermal conductivity, κ. The source terms correspond to the lorentz force in the momentum equation and the work done by the electric and magnetic fields on the fluid in the energy equation. We link the sets of equations further with the generalized Ohm's law:

$$\boldsymbol{E} + \boldsymbol{v} \times \boldsymbol{B} = \eta \boldsymbol{J}, \tag{9}$$

where the plasma resistivity, η, is the inverse of plasma conductivity, σ.

For MHD formulations we assume the modeled time scale is much greater than the time scale of the variation of the electric field; therefore, the displacement current on the right hand side of Ampere's law, Eq. (7), is negligible. This results in the elimination of electromagnetic wave propagation in the system and equates the current density, $\boldsymbol{J}$, to the curl of the magnetic field normalized by the permeability of free space, μ_0. Thus, the generalized Ohm's law can be written,

$$\boldsymbol{E} + \boldsymbol{v} \times \boldsymbol{B} = \frac{\eta}{\mu_0} \nabla \times \boldsymbol{B}, \tag{10}$$

Using Eq. (7) in the momentum source term,

$$\boldsymbol{J} \times \boldsymbol{B} = \frac{1}{\mu_0} (\nabla \times \boldsymbol{B}) \times \boldsymbol{B} = \nabla \cdot \left(\frac{1}{\mu_0} (\boldsymbol{B}\boldsymbol{B} - \frac{B^2}{2} \boldsymbol{I}) \right), \tag{11}$$

so the lorentz force can be added to the momentum flux as an additional term dependent only on the local magnetic field.

To handle the energy source term we first take the dot product of Eqs. (6) – (7) with $\boldsymbol{B}/\mu_0$ and $\boldsymbol{E}$, respectively, and subtract the two, giving,

$$\boldsymbol{E} \cdot \boldsymbol{J} + \frac{1}{\mu_0} \boldsymbol{B} \cdot \frac{\partial \boldsymbol{B}}{\partial t} = \frac{1}{\mu_0} \boldsymbol{E} \cdot (\nabla \times \boldsymbol{B}) - \frac{1}{\mu_0} \boldsymbol{B} \cdot (\nabla \times \boldsymbol{E}), \tag{12}$$

which can be rewritten and rearranged to give,

$$\boldsymbol{E} \cdot \boldsymbol{J} = -\frac{\partial}{\partial t} \left(\frac{B^2}{2\mu_0} \right) - \nabla \cdot (\frac{1}{\mu_0} \boldsymbol{E} \times \boldsymbol{B}), \tag{13}$$

where, incorporating Eq. (10),

$$\frac{1}{\mu_0} \boldsymbol{E} \times \boldsymbol{B} = \frac{1}{\mu_0} \left(\frac{\eta}{\mu_0} (\nabla \times \boldsymbol{B}) \times \boldsymbol{B} - (\boldsymbol{v} \times \boldsymbol{B}) \times \boldsymbol{B} \right) = \frac{1}{\mu_0^2} \eta \boldsymbol{B} \cdot \left((\nabla \boldsymbol{B})^{\mathrm{T}} - \nabla \boldsymbol{B} \right) - \frac{1}{\mu_0} \left((\boldsymbol{B} \cdot \boldsymbol{B}) \boldsymbol{v} - (\boldsymbol{v} \cdot \boldsymbol{B}) \boldsymbol{B} \right). \tag{14}$$

From Eq. (13) we conclude that a magnetic pressure, $B^2/(2\mu_0)$ can be added to the conserved energy density, and a new term can be added to the energy flux that is dependent on the magnetic field, defined by Eq. (14).

Lastly, the induction equation, Eq. (6), is expanded into a conservative-flux form, again using Ohm's law, Eq. (10),

$$\frac{\partial \boldsymbol{B}}{\partial t} = -\nabla \times \boldsymbol{E} = \nabla \times (\boldsymbol{v} \times \boldsymbol{B}) - \frac{1}{\mu_0}\nabla \times (\eta(\nabla \times \boldsymbol{B})) = \nabla \cdot (\boldsymbol{v}\boldsymbol{B} - \boldsymbol{B}\boldsymbol{v}) + \nabla \cdot \left(\frac{\eta}{\mu_0}\left((\nabla \boldsymbol{B})^{\mathrm{T}} - \nabla \boldsymbol{B}\right)\right). \quad (15)$$

Substituting the expanded electromagnetic source terms, and including the induction equation, results in the full set of resistive MHD equations:

$$\frac{\partial \rho}{\partial t} + \nabla \cdot (\rho \boldsymbol{v}) = 0 \quad (16)$$

$$\frac{\partial (\rho \boldsymbol{v})}{\partial t} + \nabla \cdot \left(\rho \boldsymbol{v}\boldsymbol{v} + \left(P + \frac{B^2}{2\mu_0}\right)\mathcal{I} - \boldsymbol{\tau} - \frac{1}{\mu_0}\boldsymbol{B}\boldsymbol{B}\right) = 0 \quad (17)$$

$$\frac{\partial e}{\partial t} + \nabla \cdot \left(\left(e + P + \frac{B^2}{2\mu_0}\right)\boldsymbol{v} - \boldsymbol{\tau} \cdot \boldsymbol{v} - \kappa \nabla T - \frac{1}{\mu_0}\boldsymbol{B}(\boldsymbol{v} \cdot \boldsymbol{B}) + \frac{\eta}{\mu_0^2}\boldsymbol{B} \cdot \left((\nabla \boldsymbol{B})^{\mathrm{T}} - \nabla \boldsymbol{B}\right)\right) = 0 \quad (18)$$

$$\frac{\partial \boldsymbol{B}}{\partial t} + \nabla \cdot \left((\boldsymbol{B}\boldsymbol{v} - \boldsymbol{v}\boldsymbol{B}) - \frac{\eta}{\mu_0}\left((\nabla \boldsymbol{B})^{\mathrm{T}} - \nabla \boldsymbol{B}\right)\right) = 0 \quad (19)$$

where,

$$e = \frac{P}{\gamma - 1} + \frac{1}{2}\rho v^2 + \frac{1}{2\mu_0}B^2. \quad (20)$$

2.2 Nondimensionalization

The MHD equations are nondimensionalized, with the primary purpose of eliminating the permeability of free space, μ_0, from the equations. This is done in order to allow the user to run calculations in MKS units and arrive at the same solution as they would had the calculation been run with units in which $\mu_0 = 1$, as is often the case in MHD studies. In MKS units, the user-defined initial magnetic field is normalized by $\sqrt{\mu_0}$ and the resistivity η is normalized by μ_0 (eliminating μ_0 from Eqs. (17) – (19)), the pressure is normalized by 101325 Pa, density by 1 kg/m^3, length by 1 m, and temperature by 101325/R$_u$ K where R$_u$ is the universal gas constant. The normalizations for all other variables and constants are determined in relation to these five. The normalization for temperature was chosen such that molecular weight and specific heat ratio remain unchanged under normalization. In the remainder of this paper benchmarks may use nondimensionalized or MKS units, depending on the existing literature for that benchmark; therefore, we will specify which units system is being used.

2.3 Divergence cleaning

In order to numerically enforce a divergence-free magnetic field, Eq. (5), we use the Galilean invariant, extended generalized Lagrange multiplier formulation (GIEGLM), proposed by Dedner, et al. [8]. This model was validated for the ideal MHD implementation, and its ability to numerically deal with the unphysical magnetic divergence seemlessly applies to resistive MHD as well.

We incorporate an additional conserved scalar, ϕ, with its own conservation equation and multiple gradient-based source terms. The set of resistive MHD equations in this formulation become,

$$\begin{aligned}
&\frac{\partial}{\partial t}\begin{pmatrix}\rho\\ \rho\boldsymbol{v}\\ e\\ \boldsymbol{B}\\ \phi\end{pmatrix}+\nabla\cdot\begin{pmatrix}\rho\boldsymbol{v}\\ \rho\boldsymbol{v}\boldsymbol{v}+(P_f+\frac{1}{2}|\boldsymbol{B}|^2)\mathcal{I}-\boldsymbol{B}\boldsymbol{B}\\ \boldsymbol{v}(e+P_f+\frac{1}{2}|\boldsymbol{B}|^2)-\boldsymbol{B}(\boldsymbol{v}\cdot\boldsymbol{B})\\ \boldsymbol{v}\boldsymbol{B}-\boldsymbol{B}\boldsymbol{v}+\phi\mathcal{I}\\ c_h^2\boldsymbol{B}\end{pmatrix}\\
&-\nabla\cdot\begin{pmatrix}\boldsymbol{0}\\ \boldsymbol{\tau}\\ \boldsymbol{\tau}\cdot\boldsymbol{v}+\kappa\nabla T-\eta\boldsymbol{B}\cdot\left((\nabla\boldsymbol{B})^{\mathrm{T}}-\nabla\boldsymbol{B}\right)\\ \eta\left((\nabla\boldsymbol{B})^{\mathrm{T}}-\nabla\boldsymbol{B}\right)\\ \boldsymbol{0}\end{pmatrix}=\begin{pmatrix}0\\ -(\nabla\cdot\boldsymbol{B})\boldsymbol{B}\\ -(\nabla\cdot\boldsymbol{B})\boldsymbol{v}\cdot\boldsymbol{B}-\boldsymbol{B}\cdot(\nabla\phi)\\ -(\nabla\cdot\boldsymbol{B})\boldsymbol{B}\\ -\boldsymbol{v}\cdot(\nabla\phi)-\frac{c_h^2}{c_P^2}\phi\end{pmatrix}.
\end{aligned}\tag{21}$$

Powell source terms [9], proportional to the unphysical divergence, are included, along with Dedner's extended source terms, porportional to the gradient of ϕ. The combination of the ϕ-related convective fluxes and the nonconservative source terms cause any nonzero magnetic divergence, and ϕ, to dissipate and convect with wave speeds $v \pm c_h$, where c_h is a solution-dependent value that is redefined at every time step, discussed more in Section 3.2. In this way, the scalar ϕ arises where there is nonzero magnetic divergence and facilitates the convection and dissipation of the divergence error.

2.4 DG formalism

Before presenting the DG discretization and specific numerical methods in Section 3, we formalize the derived ideal MHD equations here.

Let $\Omega \subset \mathbb{R}^d$ be a d-dimensional domain with boundary $\partial\Omega$, over which an outward normal $n : \partial\Omega \to \mathbb{R}^d$ is defined, and $T \subset \mathbb{R}^+$ is a given temporal interval. The ideal MHD equations, Eqs. (16) – (19), defined in strong form for piecewise smooth, $\mathbb{R}^m$-valued functions y, with gradient ∇y, are given as

$$\frac{\partial y}{\partial t} + \nabla \cdot \mathcal{F}(y, \nabla y) - \mathcal{S}(y, \nabla y) = 0 \text{ in } \Omega \times T, \tag{22}$$

$$y(\cdot, t_0) - y_0 = 0 \text{ in } \Omega, \tag{23}$$

$$n \cdot \mathcal{F}(y, \nabla y) - n \cdot \mathcal{F}_\partial(y, \nabla y) = 0 \text{ on } \partial\Omega \times T, \tag{24}$$

$$G_\partial(y_\partial) : (y^+ - y_\partial) \otimes n = 0 \text{ on } \partial\Omega \times T, \tag{25}$$

where t denotes time, $\mathcal{F} : \mathbb{R}^m \to \mathbb{R}^{m \times d}$ is a known flux function, and $\mathcal{S} : \mathbb{R}^m \to \mathbb{R}^m$ is a known source term that may be a function of the the gradient of the state. The initial conditions at time t_0 are given by y_0. The flux function

$$\mathcal{F}(y, \nabla y) = \mathcal{F}^c(y) - \mathcal{F}^v(y, \nabla y) \tag{26}$$

is defined in terms of the convective flux $\mathcal{F}^c(y)$, which is only a function of the state y, and the viscous flux $\mathcal{F}^v(y, \nabla y)$, which is a function of the state and the state gradient. This viscous flux can be written as

$$\mathcal{F}^v(y, \nabla y) = G(y) : \nabla y \tag{27}$$

where $G(y) = \mathcal{F}^v_{\nabla y}$ is the partial linearization with respect to the state gradient, otherwise known as the homogeneity tensor [10].

The boundary conditions given by Eq. (24) are enforced through the boundary flux, $\mathcal{F}_\partial(y, \nabla y) = \mathcal{F}^c_\partial(y) - \mathcal{F}^v_\partial(y, \nabla y)$, where $\mathcal{F}^c_\partial(y)$ and $\mathcal{F}^v_\partial(y, \nabla y)$ are the convective and viscous fluxes, respectively, at the boundary. The condition on the state at the boundary given by Eq. (25) is impose through the boundary state y_∂ and the boundary-modified homogeniety tensor, $G_\partial(y_\partial)$.

The GIEGLM resistive MHD flow state variable is given by

$$y = (\rho, \rho v_1, \rho v_2, \rho v_3, e, B_1, B_2, B_3, \phi), \tag{28}$$

where the velocity and magnetic field vectors, $\boldsymbol{v}$ and $\boldsymbol{B}$, always have three components, such that $m = 9$. The k-th spatial convective flux component is given by

$$\mathcal{F}_k^c(y) = \begin{pmatrix} \rho v_k \\ \rho v_1 v_k + P_t \delta_{k1} - B_k B_1 \\ \rho v_2 v_k + P_t \delta_{k2}, -B_k B_2 \\ \rho v_3 v_k + P_t \delta_{k3} - B_k B_3 \\ v_k(e + P_t) - B_k(\boldsymbol{v} \cdot \boldsymbol{B}) \\ v_k B_1 - v_1 B_k + \phi \delta_{k1} \\ v_k B_2 - v_2 B_k + \phi \delta_{k2} \\ v_k B_3 - v_3 B_k + \phi \delta_{k3} \\ c_h^2 B_k \end{pmatrix}, \tag{29}$$

where the total pressure, $P_t = P + B^2/(2\mu_0)$ is the sum of the fluid dynamic and magnetic pressures. The k-th spatial viscous flux component is given by

$$\mathcal{F}_k^v(y, \nabla y) = \begin{pmatrix} 0 \\ \tau_{1k} \\ \tau_{2k} \\ \tau_{3k} \\ \tau_k \cdot \boldsymbol{v} + \kappa \frac{\partial T}{\partial x_k} - \boldsymbol{B} \cdot \mathrm{T}_k \\ \mathrm{T}_1 k \\ \mathrm{T}_2 k \\ \mathrm{T}_3 k \\ 0 \end{pmatrix}, \tag{30}$$

where $\mathrm{T} : \mathbb{R}^m \times \mathbb{R}^{m \times d} \to \mathbb{R}^{d \times d}$ is an antisymmetric magnetic tensor with k-th spatial component given by

$$\mathrm{T}_k(y, \nabla y) = \eta \left(\frac{\partial B_1}{\partial x_k} - \frac{\partial B_k}{\partial x_1}, \frac{\partial B_2}{\partial x_k} - \frac{\partial B_k}{\partial x_2}, \frac{\partial B_3}{\partial x_k} - \frac{\partial B_k}{\partial x_3} \right). \tag{31}$$

The k-th spatial component of the viscous stress tensor is given by

$$\tau_k(y, \nabla y) = \mu \left(\frac{\partial v_1}{\partial x_k} + \frac{\partial v_k}{\partial x_1} - \delta_{k1} \frac{2}{3} \nabla \cdot \boldsymbol{v}, \frac{\partial v_2}{\partial x_k} + \frac{\partial v_k}{\partial x_2} - \delta_{k2} \frac{2}{3} \nabla \cdot \boldsymbol{v}, \frac{\partial v_3}{\partial x_k} + \frac{\partial v_k}{\partial x_3} - \delta_{k3} \frac{2}{3} \nabla \cdot \boldsymbol{v} \right). \tag{32}$$

The source term for the GIEGLM formulation is given by

$$\mathcal{S}(y,\nabla y) = \begin{pmatrix} 0 \\ -(\nabla\cdot\boldsymbol{B})\boldsymbol{B} \\ -(\nabla\cdot\boldsymbol{B})\boldsymbol{v}\cdot\boldsymbol{B} - \boldsymbol{B}\cdot(\nabla\phi) \\ -(\nabla\cdot\boldsymbol{B})\boldsymbol{B} \\ -\boldsymbol{v}\cdot(\nabla\phi) - \frac{c_h^2}{c_p^2}\phi \end{pmatrix}. \tag{33}$$

Throughout this work the ratio of specific heats, γ, and the plasma molecular weight, $\mathcal{M}$, are constant. The transport properties are also constant and specified in each case by setting the plasma conductivity, $\sigma = 1/\eta$, dynamic viscosity, μ, and Prandtl number, $\text{Pr} = c_p\mu/\kappa$, where $c_p = \gamma R_u/(\mathcal{M}(\gamma-1))$ is the constant pressure specific heat. The thermal conductivity, κ, is determined from Pr.

3. FORMULATION

Assume the domain Ω is partitioned by $\mathcal{T}$, made up of discrete cells κ, with interfaces ϵ composing a set $\mathcal{E}$, over which an oriented normal $n : \epsilon \to \mathbb{R}^d$ is defined. Also assume that $\mathcal{E}$ consists of two disjoint subsets: the interior interfaces $\epsilon_\mathcal{I} \in \mathcal{E}_\mathcal{I}$ and the exterior interfaces $\epsilon_\partial \in \mathcal{E}_\partial$. For interior interfaces there exists $\kappa^+, \kappa^- \in \mathcal{T}$ such that $\epsilon_\mathcal{I} = \partial\kappa^+ \bigcap \partial\kappa^-$ and n^+, n^- are outward facing normals of κ^+, κ^-, respectively. Lastly, assume that there is a continuous invertible mapping, $u : \hat{\Omega} \to \Omega$, from reference domain $\hat{\Omega} \subset \mathbb{R}^d$ to the physical domain $\Omega \subset \mathbb{R}^d$ [11].

Now, we use a discrete subspace V_h^p over $\mathcal{T}$ of piecewise polynomials. Let $\mathcal{P}_p$ be the space of polynomials spanned by the monomials $\boldsymbol{x}^\alpha$ with multi-index $\alpha \in \mathbb{N}_0^d$, satisfying $\alpha_i \leq p$ for $i = 1, ..., d$. Then,

$$V_h^p = \left\{ v \in \left[L^2(\Omega)\right]^m \middle| \forall \kappa \in \mathcal{T}, v|_\kappa \circ u \in \left[\mathcal{P}_p\right]^m \right\}. \tag{34}$$

3.1 Discretization

The DG (semi-)discretization of Eqs. (22) – (24) is defined as: find $\frac{\partial y}{\partial t} \in V_h^p$ such that

$$\begin{aligned} &\sum_{\kappa\in\mathcal{T}} \left(\frac{\partial y}{\partial t}, v\right)_\kappa - \sum_{\kappa\in\mathcal{T}} \left(\mathcal{F}(y,\nabla y), \nabla v\right)_\kappa + \sum_{\epsilon\in\mathcal{E}} \left(h(y,n), [\![v]\!]\right)_\mathcal{E} - \sum_{\epsilon\in\mathcal{E}} \left(\{\{\mathcal{F}^v(y,\nabla y)\}\}\cdot n - \delta(y,n), [\![v]\!]\right)_\mathcal{E} \\ &+ \sum_{\kappa\in\mathcal{T}} \left(G(y^+) : (\{\{y\}\} - y^+ \otimes n, \nabla v)\right)_{\partial\kappa} - \sum_{\kappa\in\mathcal{T}} \left(\mathcal{S}(y, \nabla y - L_0(y)), v\right)_\kappa = 0 \quad \forall v \in V_h^p \text{ and } \forall t \in T, \end{aligned} \tag{35}$$

where $(\cdot,\cdot)$ denotes the inner product, $h(y,n)$ is the numerical flux, $\delta(y,n)$ is a penalty term that is required for stability, $[\![\cdot]\!]$ denotes the jump operator, $\{\{\cdot\}\}$ denotes the average operator, and $L_0(y)$ is a global lifting operator, defined in Section 3.3. The numerical flux used in this work is a Roe-type flux for MHD [12],

explained more in our prior work [7] and in the Athena code documentation [13]. The penalty term δ is implemented via the modified formulation of Bassi and Rebay [14–16], known as BR2.

The discrete solution is given by the coefficients of a nodal basis defined for each element at the Guass-Lobatto points of that element. The volume and surface terms of Eq. (35) are numerically evaluated with a quadrature free method [17].

On interior interfaces, $\mathcal{E}_I$, the jump, average, numerical flux, and penalty term are defined as

$$[\![v]\!] = v^+ - v^- \text{ on } \epsilon \quad \forall \epsilon \in \mathcal{E}_I, \tag{36}$$

$$\{\{y\}\} = \frac{1}{2}(y^+ + y^-) \text{ on } \epsilon \quad \forall \epsilon \in \mathcal{E}_I, \tag{37}$$

$$\{\{\mathcal{F}^v(y, \nabla y)\}\} = \frac{1}{2}(\mathcal{F}^v(y^+, \nabla y^+) + \mathcal{F}^v(y^-, \nabla y^-)) \text{ on } \epsilon \quad \forall \epsilon \in \mathcal{E}_I, \tag{38}$$

$$h(y, n) = h(y^+, y^-, n) \text{ on } \epsilon \quad \forall \epsilon \in \mathcal{E}_I, \tag{39}$$

$$\delta(y, n) = \delta(y^+, y^-, n) \text{ on } \epsilon \quad \forall \epsilon \in \mathcal{E}_I. \tag{40}$$

On the exterior interfaces, $\mathcal{E}_\partial$, they are defined as

$$[\![v]\!] = v^+ \text{ on } \epsilon \quad \forall \epsilon \in \mathcal{E}_\partial, \tag{41}$$

$$\{\{y\}\} = y_\partial(y^+, n^+) \text{ on } \epsilon \quad \forall \epsilon \in \mathcal{E}_\partial, \tag{42}$$

$$\{\{\mathcal{F}^v(y, \nabla y)\}\} = \mathcal{F}^v_\partial(y_\partial(y^+, n^+), \nabla y^+) \text{ on } \epsilon \quad \forall \epsilon \in \mathcal{E}_\partial, \tag{43}$$

$$h(y, n) = h_\partial(y^+, n^+) \text{ on } \epsilon \quad \forall \epsilon \in \mathcal{E}_\partial, \tag{44}$$

$$\delta(y, n) = \delta_\partial(y^+, n^+) \text{ on } \epsilon \quad \forall \epsilon \in \mathcal{E}_\partial, \tag{45}$$

where $y_\partial(y^+, n^+)$ is the prescribed boundary state, $h_\partial(y^+, n^+)$ is the numerical boundary flux, and $\mathcal{F}^v_\partial(y_\partial(y^+, n^+), \nabla y^+)$ is the viscous boundary flux.

In this work we use the following boundary conditions, where the k-th spatial component of the viscous boundary flux is denoted $\mathcal{F}^v_{\partial,k}(y_\partial(y^+, n^+), \nabla y^+)$, and the boundary stress tensor, $\tau_\partial = \tau(y_\partial(y^+, n^+), \nabla y^+)$ and boundary magnetic tensor, $\mathrm{T}_\partial = \mathrm{T}(y_\partial(y^+, n^+), \nabla y^+)$, are both evaluated at the boundary state and the interior gradient.

Inflow:

$$y_\partial(y^+, n^+) = y_\infty \text{ on } \epsilon \quad \forall \epsilon \in \mathcal{E}_{\text{in}}, \tag{46}$$

$$\mathcal{F}^v(y_\partial(y^+, n^+), \nabla y^+) = \mathcal{F}^v_k(y_\infty, \nabla y^+) \text{ on } \epsilon \quad \forall \epsilon \in \mathcal{E}_{\text{in}}, \tag{47}$$

$$h_\partial(y^+, n^+) = \mathcal{F}^c(y_\infty) \cdot n^+ \text{ on } \epsilon \quad \forall \epsilon \in \mathcal{E}_{\text{in}}, \tag{48}$$

$$\delta_\partial(y^+, n^+) = \delta(y^+, y_\infty) \text{ on } \epsilon \quad \forall \epsilon \in \mathcal{E}_{\text{in}}, \tag{49}$$

where $y_\infty : \Omega \to \mathbb{R}^m$ is a prescribed state.

Ouflow:

At an outflow boundary condition the boundary state is entirely defined by the interior state, therefore it is given by

$$y_\partial(y^+, n^+) = y_+ \text{ on } \epsilon \quad \forall \epsilon \in \mathcal{E}_{\text{in}}, \tag{50}$$
$$\mathcal{F}^v(y_\partial(y^+, n^+), \nabla y^+) = \mathcal{F}^v_k(y^+, \nabla y^+) \text{ on } \epsilon \quad \forall \epsilon \in \mathcal{E}_{\text{in}}, \tag{51}$$
$$h_\partial(y^+, n^+) = \mathcal{F}^c(y_+) \cdot n^+ \text{ on } \epsilon \quad \forall \epsilon \in \mathcal{E}_{\text{in}}, \tag{52}$$
$$\delta_\partial(y^+, n^+) = 0 \text{ on } \epsilon \quad \forall \epsilon \in \mathcal{E}_{\text{in}}, \tag{53}$$

Conducting, slip wall:

At a conducting, slip wall, the flow and the magnetic field are required to be parallel to the boundary. We define the boundary velocity, $(v_{\partial,1}, v_{\partial,2}, v_{\partial,3}) : \mathbb{R}^m \times \mathbb{R}^d \to \mathbb{R}^d$ as

$$\boldsymbol{v}_\partial(y^+, n^+) = \left(v_1^+ - \left(\sum_{k=1}^{3} v_k^+ n_k^+ \right) n_1^+, v_2^+ - \left(\sum_{k=1}^{d} v_k^+ n_k^+ \right) n_2^+, v_3^+ - \left(\sum_{k=1}^{d} v_k^+ n_k^+ \right) n_3^+ \right), \tag{54}$$

and the boundary magnetic field as,

$$\boldsymbol{B}_\partial(y^+, n^+) = \left(B_1^+ - \left(\sum_{k=1}^{3} B_k^+ n_k^+ \right) n_1^+, B_2^+ - \left(\sum_{k=1}^{d} B_k^+ n_k^+ \right) n_2^+, B_3^+ - \left(\sum_{k=1}^{d} B_k^+ n_k^+ \right) n_3^+ \right), \tag{55}$$

where the normal components have been set to zero. The boundary condition is specified as

$$y_\partial(y^+, n^+) = (\rho^+, \rho^+ v_{\partial,1}, \rho^+ v_{\partial,2}, \rho^+ v_{\partial,3}, e^+, B_{\partial,1}, B_{\partial,2}, B_{\partial,3}, \phi) \text{ on } \epsilon \quad \forall \epsilon \in \mathcal{E}_{\text{in}}, \tag{56}$$
$$\mathcal{F}^v(y_\partial(y^+, n^+), \nabla y^+) = (\tau_{\partial,1k}, \tau_{\partial,2k}, \tau_{\partial,3k}, \tau_{\partial,k} \cdot \boldsymbol{v}_\partial - \boldsymbol{B}_\partial \cdot \mathrm{T}_{\partial,k}, \mathrm{T}_{\partial,1k}, \mathrm{T}_{\partial,2k}, \mathrm{T}_{\partial,3k}, 0) \text{ on } \epsilon \quad \forall \epsilon \in \mathcal{E}_{\text{in}}, \tag{57}$$
$$h_\partial(y^+, n^+) = h(y^+, 2y_\partial(y^+, n^+) - y^+, n^+) \text{ on } \epsilon \quad \forall \epsilon \in \mathcal{E}_{\text{in}}, \tag{58}$$
$$\delta_\partial(y^+, n^+) = \delta(y^+, y_\partial(y^+, n^+)) \text{ on } \epsilon \quad \forall \epsilon \in \mathcal{E}_{\text{in}}, \tag{59}$$

where we have required that the thermal heat flux be zero. The viscous flux is computed from the boundary state and the interior gradient, while the numerical flux is evaluated at the interior state and the reflected state, $2y_\partial(y^+, n^+) - y^+$, following Hartmann and Leicht [10].

Insulating, adiabatic wall:

At an insulating, adiabatic wall, the flow moves at a specified wall velocity (often zero), the boundary-tangential component of the magnetic field is set to zero, and the thermal heat flux is set to zero. The boundary condition is given as

$$y_\partial(y^+, n^+) = (\rho^+, \rho^+ v_{\partial,1}, \rho^+ v_{\partial,2}, \rho^+ v_{\partial,3}, e^+, B_{\partial,1}, B_{\partial,2}, B_{\partial,3}, \phi) \text{ on } \epsilon \quad \forall \epsilon \in \mathcal{E}_{\text{in}}, \tag{60}$$

$$\mathcal{F}^v(y_\partial(y^+, n^+), \nabla y^+) = (\tau_{\partial,1k}, \tau_{\partial,2k}, \tau_{\partial,3k}, \tau_{\partial,k} \cdot \boldsymbol{v}_\partial - \boldsymbol{B}_\partial \cdot \mathrm{T}_{\partial,k}, \mathrm{T}_{\partial,1k}, \mathrm{T}_{\partial,2k}, \mathrm{T}_{\partial,3k}, 0) \text{ on } \epsilon \quad \forall \epsilon \in \mathcal{E}_{\text{in}}, \tag{61}$$

$$h_\partial(y^+, n^+) = \mathcal{F}^c(y_\partial(y^+, n^+)) \cdot n^+ \text{ on } \epsilon \quad \forall \epsilon \in \mathcal{E}_{\text{in}}, \tag{62}$$

$$\delta_\partial(y^+, n^+) = \delta(y^+, y_\partial(y^+, n^+)) \text{ on } \epsilon \quad \forall \epsilon \in \mathcal{E}_{\text{in}}, \tag{63}$$

where $(v_{\partial,1}, v_{\partial,2}, v_{\partial,3}) : \Omega \to \mathbb{R}^d$ is the prescribed boundary velocity, and the boundary magnetic field is defined as

$$\boldsymbol{B}_\partial(y^+, n^+) = \left(\left(\sum_{k=1}^{3} B_k^+ n_k^+ \right) n_1^+, \left(\sum_{k=1}^{3} B_k^+ n_k^+ \right) n_2^+, \left(\sum_{k=1}^{3} B_k^+ n_k^+ \right) n_3^+ \right). \tag{64}$$

3.2 Integration parameters

Equation (35) is integrated temporally with a second order strong-stability-preserving Runge-Kutta method, with a time step that is restricted by the Courant-Friedrichs-Lewy (CFL) number, defined as

$$\mathrm{CFL} = \frac{\Delta t}{(2p+1)\min(\Delta x)} \lambda_{\max}, \tag{65}$$

where $\lambda_{\max}$ is the fastest wave speed [7].

The constants c_h and c_p introduced in Eq. (21) as part of the GIEGLM formulation are spatially constant but are free to change each time step. We follow Derigs, et al. [18] and restrict the divergence wave speed,

$v \pm c_h$, from exceeding the maximum wave speed, so as not to interfere with the CFL criterion. This is enforced by

$$c_h = \lambda_{\max} - v_{\max,\Omega}, \tag{66}$$

where $v_{\max,\Omega} = \max_\Omega(|v_1|, |v_2|, |v_3|)$ is the greatest fluid speed in the domain. The divergence dissipation parameter c_p is prescribed such that the ratio $c_r = c_p^2/c_h = 0.18$ at all times.

3.3 Nonconservative source terms

For the nonconservative, gradient sources in the GIEGLM, Eq. (21), the source term discretization in Eq. (35) requires the global lifting operator [19],

$$L_0(y) = \sum_{\epsilon \in \mathcal{E}} L_0^\epsilon(y), \tag{67}$$

defined in terms of the local lifting operator,

$$(L_0^\epsilon(y), \tau)_\kappa = (\llbracket y \otimes n \rrbracket, \{\{\tau\}\})_\epsilon \quad \forall \tau \in \Sigma_h^p, \tag{68}$$

where $\Sigma_h^p = \left[V_h^p\right]^2$ is the space of vector-valued discontinuous piecewise polynomial functions of degree $p \geq 0$ [20].

A key finding in the prior report was that the lifting operator is required in order to see the correct propagation of the magnetic divergence in the GIEGLM formulation. This is because the propagation wave speeds with a local velocity component are not dependent explicitly on the convective fluxes; rather, they are enforced and arise through the proper determination and integration of the divergence source terms.

4. RESULTS

To demonstrate the efficacy of the resistive MHD implementation, we present a series of benchmarks in one and two dimensions. The chosen cases test the physical, resistive diffusion in particular, as opposed to the viscous and thermal diffusion implemented, since those aspects of the JENRE® code, though present in some of these benchmarks, have been validated elsewhere [11, 21].

4.1 Self-similar current sheet

We consider a one-dimensional current sheet, in which B_z begins as a step function around $x = 0$, defined by,

$$B_z(x) = \begin{cases} -B_0 & x < 0 \\ B_0 & x \geq 0 \end{cases}, \tag{69}$$

in nondimensionalized units. Under resistive diffusion, the infinitesimal current sheet will undergo magnetic reconnection as the discontinuous magnetic field diffuses together. Isolated from convective fluxes, this diffusion event has a self-similar, analytical solution, given by,

$$B_z(x,t) = B_0 \text{erf}\left(\frac{x}{\sqrt{4\eta t}}\right), \tag{70}$$

where $\text{erf}(\cdot)$ is the error function.

Thus, we turn off convective fluxes for this case and consider only resistive diffusion for a resistivity $\eta = 0.01$. Viscosity is ignored ($\mu = 0$), $\gamma = 1.4$, $B_0 = 1$, and the fluid pressure and density are set to $P = 50$ and $\rho = 1$, respectively. We initialize the case with the magnetic profile at time $t = 0.5$ in Eq. (70) so that we are considering only the error due to the diffusive flux implementation and not from the large discontinuity across cells that would be present at time $t = 0$.

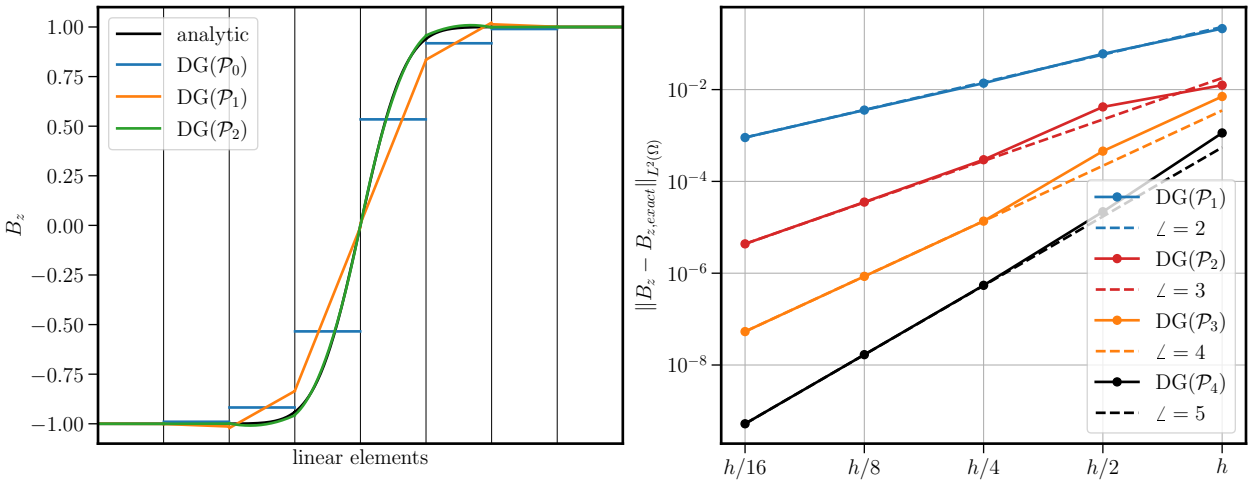

Fig. 1—1D self-simlar current sheet at t = 5.5, (left) comparing the final analytical solution to that of various order elements on an 8-element mesh and (right) showing convergence of the B_z profile with $h-$refinement for different order elements

Figure 1 shows the results at time $t = 5.5$ for various orders of accuracy and spatial resolution. On the left we see the convergence of the numerical solution under polynomial (p) refinement. For polynomial

degree $p = 2$, the solution is almost indistinguishable from the analytical on just 8 piecewise-quadratic elements. The right shows the convergence under grid (h) refinement for polynomial degrees $p = 1$, 2, 3, and 4 along with the theoretical rates of convergence. We see very good agreement with theory for both h and p refinement in this one-dimensional case.

4.2 Resistive diffusion

As in the previous case, we isolate the resistive diffusion from convective fluxes, now in a two dimensional domain with a sinusoidal profile in the magnetic field, given by,

$$B_z(x, y) = B_0 \sin(2\pi x) \sin(2\pi y) \tag{71}$$

where B_0 is the peak, nondimensionalized magnetic field. The analytical solution for the resistive diffusion is,

$$B_z(x, y, t) = B_0 \sin(2\pi x) \sin(2\pi y) \mathrm{e}^{-2\eta t (2\pi)^2}. \tag{72}$$

We initialize a triangular element domain defined by $0 < x < 1$, $0 < y < 1$, at time $t = 0$ with resistivity, $\eta = 0.01$, no viscosity, $\mu = 0$, $\gamma = 1.4$, $P = 50$, and $\rho = 1$. The case was run for various grid resolutions for polynomial degrees $p = 1$, 2, and 3 until time $t = 0.05$ with a constant time step, $dt = 10^{-6}$. This time step was chosen to keep the temporal error significantly smaller than the spatial error at all resolutions and polynomial values, so as to not affect the rates of convergence.

Figure 2 shows the L^2-errors of B_z at time $t = 0.05$ with the expected rates of convergence. This shows good agreement with theory, validating the resistive diffusion implementation in multiple dimensions.

4.3 Magnetic reconnection

It is crucial for any resistive MHD model to capture multi-dimensional magnetic reconnection, particularly the formation or supression of magnetic islands along a current sheet. With sufficient resistivity, the diffusion of the magnetic field supresses the formation of magnetic islands and allows for a more smooth, less energetic magnetic reconnection event. The present case evaluates the ability of our implementation to capture this effect. For this we use a common configuration [22, 23] that has an approximate analytical model produced by Sweet [24] and Parker [25].

The Sweet-Parker model defines the rate of magnetic reconnection as the ratio of fluid velocity flowing into the reconnection layer to the fluid velocity flowing out which, by conservation of mass, is approximately equal to the ratio of the reconnection layer width to length:

$$\epsilon \equiv \frac{u_{\text{in}}}{u_{\text{out}}} \approx \frac{\delta}{L}, \tag{73}$$

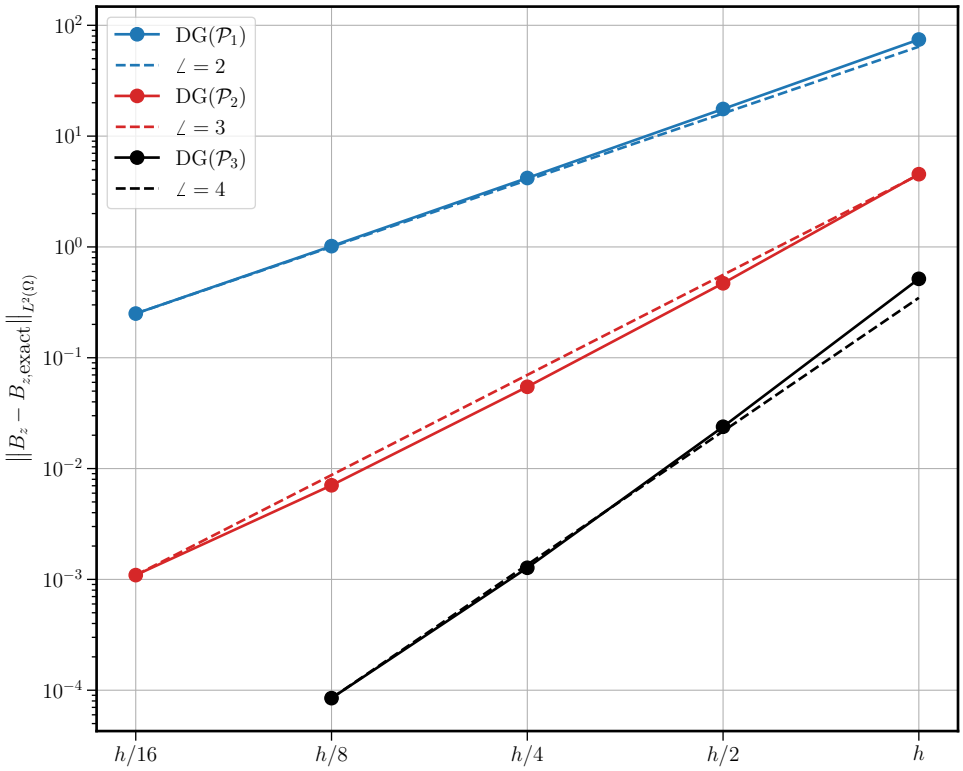

Fig. 2—2D resistive diffusion of a sinusoidal profile at t = 0.05, showing convergence of the B_z profile with $h-$refinement for different order elements

where δ and L are the layer width and length, respectively. The model balances the convective flow with ohmic diffusion by setting, in nondimensional units, $u_{\text{in}} = \eta/\delta$, for resistivity η, and u_{out} equal to the Alfvén velocity, $v_A = B/\sqrt{\rho}$. Defining the Lundquist number as $S \equiv Lv_A/\eta$, and therefore $\eta/v_A = L/S$, leads to,

$$\epsilon \approx \frac{\delta}{L} \propto \eta^{1/2}. \tag{74}$$

This relation is called the Sweet-Parker scaling and provides a predicted trend in the aspect ratio of the reconnection layer.

Our simulations are run in a rectangular domain defined on $x \in [-L_x/2, L_x/2]$ and $y \in [-L_y/2, L_y/2]$, with initial conditions given by $P = 0.5$, $\rho = \rho_\infty + \rho_0 \text{sech}(y/\lambda)$, $B_x = B_o \tanh(y/\lambda)$, and velocity zero everywhere. The magnetic fields are perturbed by

$$\delta B_x = -\pi\psi_0/L_y \sin(\pi y/L_y)\cos(2\pi x/\text{L}_x), \tag{75}$$

$$\delta B_y == 2\pi\psi_0/L_x \sin(2\pi x/L_x)\cos(\pi y/\text{L}_y). \tag{76}$$

For all cases we use $(L_x, L_y) = (25.6, 12.8)$, initial layer thickness $\lambda = 0.5$, background density $\rho_\infty = 0.2$, $\rho_0 = 1.0$, an initial magnetic field strength of $B_0 = 1.0$, a perturbation size of $\psi_0 = 0.1$, and an adiabatic index of $\gamma = 1.4$.

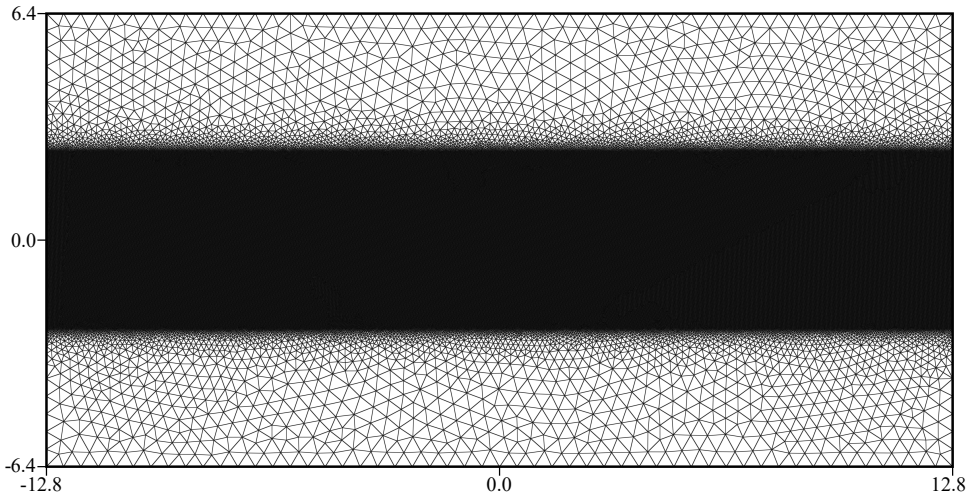

Fig. 3—495,000 triangular-element mesh used for the magnetic reconnection benchmark on a 25.6 x 12.8 domain

The computational mesh is shown in Fig. 3 with approximately 495,000 triangular elements. The mesh is more resolved along $y = 0$ in the center third of the vertical axis with minimum element size 0.025. The left and right boundaries are periodic, and the top and bottom boundaries are reflective, slip walls. The course elements on the top and bottom dissipate acoustic perturbations propagating out of the area of interest and act to mitigate the strength of the disturbances reflecting back to the center. We vary plasma conductivity, and therefore resistivity, between cases and run each case to time $t = 50$.

The fluid pressure at the final time is presented in Fig. 4 for three cases ($\sigma = 100, 250, 1000$). In all cases the perturbed current sheet forms magnetic islands on the vertical boundaries which then diffuse together at the center of the domain. The effect that resistivity has on the rate of reconnection and the structure of the reconnection layer is evident. As resistivity is increased (conductivity decreased) the convective structures are smeared and the reconnection of opposing magnetic field lines occurs more quickly. In the case of minimum resistivity considered, a secondary island begins to form by the end of the simulation time. This exhibits a tearing mode instability described by Biskamp [26] that occurs for large aspect ratios, L/δ. This is driven by the dominance of convective forces over resistive forces as the transport parameters approach that of ideal MHD ($\eta \to 0$).

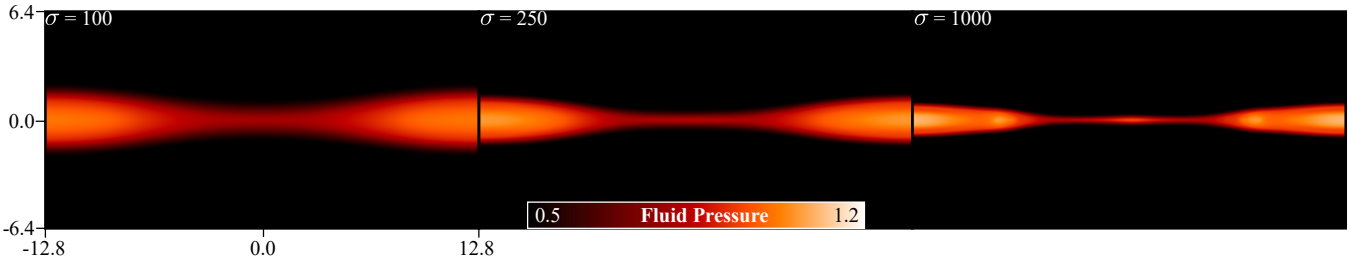

Fig. 4—fluid pressure comparison at $t = 50$ for magnetic reconnection with various plasma conductivities

We further evaluate the effect of resistivity by comparing against the Sweet-Parker scaling, Eq. (74). For each case the reconnection layer's half-width and half-length are approximated by the e-folding distance of the current density from the center of the domain in the vertical and horizontal directions, respectively. These distances are time-averaged for each case, and the ratios are plotted in Fig. 5 against the square root of the resistivity for the five values for which the simulation was run. A regression line is plotted with the computed reconnection rates. With an R-value of 0.9983, we see a strong linear relation between the approximate rate of reconnection and the square root of the magnetic resistivity. This provides quantitative validation of the resistive MHD implementation against the Sweet-Parker model for resistive reconnection.

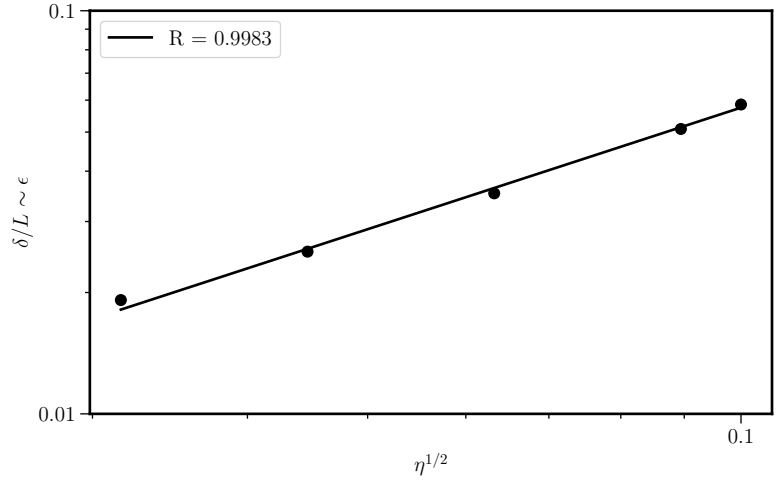

Fig. 5—linear trend for the rate of reconnection as a function of the square root of the resistivity

4.4 MHD Rayleigh problem

Our final benchmark is the case of a semi-infinite flat plate impulsively set in motion in an electrically conducting fluid with a magnetic field perpendicular to the direction of motion. If the plate is perfectly insulated, a Hartmann layer will form in the magnetic field near the plate, along with a fluid boundary layer, since the normal component of the magnetic field vanishes at the plate surface. The sudden motion of the plate also propagates a plane Alfvén wave into the quescient fluid, behind which the fluid is in motion. The Alfvén wave also perturbs the imposed magnetic field, inducing a nonzero field perpendicular to the direction of wave travel (the x-direction). When the fluid's kinematic viscosity is equal to the magnetic diffusivity the fluid has a unity magnetic Prandtl number, Pr_m. In this case, the Hartmann layer and fluid viscous boundary layer have the same thickness, and there exists an analytical solution [27], making this MHD Rayleigh problem a useful and popular benchmark for resistive MHD models [28, 29].

The analytical solution is given by

$$v_x(y,t) = \frac{U}{4}(2 - (\mathrm{erf}\lambda_+ + \mathrm{erf}\lambda_-) + \mathrm{e}^{-v_{A,0}y/d}(1 - \mathrm{erf}\lambda_-) + \mathrm{e}^{v_{A,0}y/d}(1 - \mathrm{erf}\lambda_+)), \tag{77}$$

$$a_x(y,t) = \frac{U}{4}((\mathrm{erf}\lambda_- - \mathrm{erf}\lambda_+) + \mathrm{e}^{-v_{A,0}y/d}(1 - \mathrm{erf}\lambda_-) - \mathrm{e}^{v_{A,0}y/d}(1 - \mathrm{erf}\lambda_+)), \tag{78}$$

where

$$\lambda_{\pm} = \frac{y \pm v_{A,0} t}{2\sqrt{dt}}, \tag{79}$$

$$d = \nu = \eta, \tag{80}$$

$$a_x = \frac{B_x}{\sqrt{\mu_0 \rho}}. \tag{81}$$

For this case we use MKS units, hence the presence of μ_0 in Eq. (81), so the Alfvén wave speed in the analytical solution is defined by $v_{A,0} = B_0/\sqrt{\mu_0 \rho}$, with respect to initial magnetic field strength, B_0. We set plasma conductivity $\sigma = (10^7/(4\pi))(\Omega\text{m})^{-1}$, dynamic viscosity $\mu = 4 \times 10^{-5}$ Pa s, and fluid density $\rho = 4 \times 10^{-5}$ kg/m^3. This ensures a unity magnetic Prandtl number, $\text{Pr}_m = \mu\sigma\mu_0/\rho = 1$. From a frame of rest, the plate is moving to the left at a speed of 1 m/s, the adiabatic index is 1.4, and the magnetic field is in the positive y-direction with a strength of $B_0 = 1.4494 \times 10^{-4}$ Tesla. This sub-magnetosonic flow corresponds to a magnetic Reynolds number of 1, with respect to a unity length scale. The acoustic sound speed is 614.6 m/s, while the Alfvén wave speed tangential to the initial magnetic field is just 20.4 m/s.

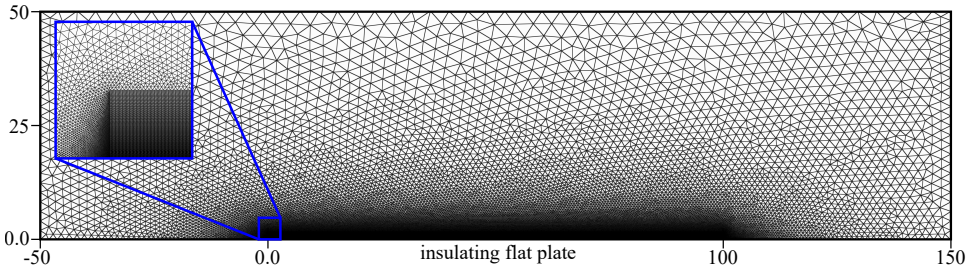

Fig. 6—275,000 triangular-element mesh used for the MHD Rayleigh problem on a 200 x 50 m domain, with an inset expansion of a 5 x 5 region around the boundary layer elements

The computational mesh is shown in Fig. 6. The simulated flat plate is centered on the bottom boundary of the domain, with a more resolved boundary layer mesh than elsewhere in the domain. The zoomed overlay reveals a structured boundary layer mesh with stretched triangular elements, surrounded by an unstructured mesh that becomes progressively less resolved away from the region of interest. The flat plate is modeled as an insulated, adiabatic wall defined by Eqs. (60) – (63), while the remainder of the bottom boundary (upstream and downstream of the flat plate) and the top boundary are slip walls. The left and right boundaries are inflow and outflow conditions, respectively. The left, right, and top boundaries are placed a distance of 50 m from the flat plate, corresponding to the distance traveled in the simulated time by sound waves induced by the impulsive motion of the plate. This was done to avoid the need for characteristic or subsonic inflow/outflow boundary conditions, which would be required at these surfaces if they were to interact with these pressure waves. This choice of dimension, the length of the flat plate, and the placement of the line probe at the center of the flat plate enables proper simulation of a semi-infinite flat plate.

The probed simulation results are shown in Fig. 7 at various simulation times along with the analytical solutions for the x-components of the velocity and magnetic field. The simulation agrees very well with

theory. The Hartmann layer in the magnetic field and the boundary layer in the velocity are clearly seen near the wall with the same thickness, as is expected with a unity magnetic Prandtl number. The Alfvén wave front is seen propagating upward at the correct rate in the magnetic field and velocity, inducing profiles that plateau at the perturbed values.

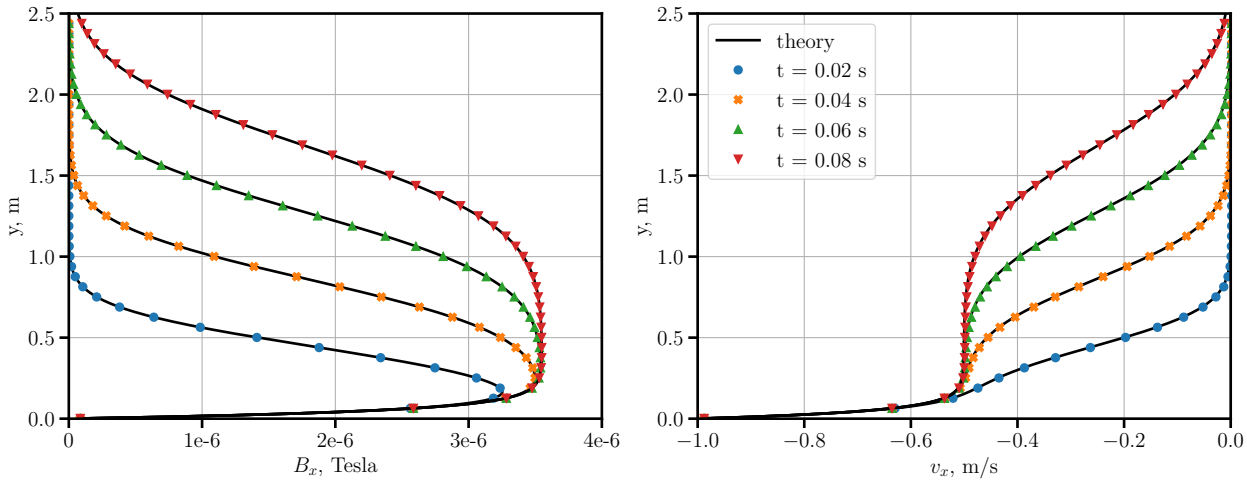

Fig. 7—(left) induced B_x and (right) v_x for the MHD rayleigh problem at times t = 0.02, 0.04, 0.06, and 0.08 s, compared with the cooresponding theoretical solutions [30]

The accuracy of our numerical solution to the MHD Rayleigh problem carries significant weight in validating the implementation and capability of the resistive MHD solver. This highly viscous and resistive regime, and the Hartmann layer that emerges, can only be captured by a solver that accurately models the diffusive fluxes and appropriately handles an insulating, no-slip boundary condition.

5. FUTURE WORK

With the goal of developing MHD modeling capabilities that can be used to study the interaction of hypersonic flows with electromagnetic fields, resistive MHD is an important extension past ideal MHD. With this functionality we can model diffusion-dominated flowfields such as those arising in a weakly ionized, nonequilibrium plasma around a hypersonic vehicle traveling through the Earth's magnetic field. The effect of a naturally-occuring or intentially-applied magnetic field on such a flow could never be modeled without consideration of the resistive diffusion of the magnetic field throughout the fluid. In this way, the present work is crucial in bringing about this desired capability. However, there are additional model developments and numerical implementations that, if pursued, lend themselves nicely to the types of systems we aim to consider. These should be the focus of future work.

One such formulation involves splitting the magnetic field into a constant, applied magnetic field and a time-dependent, induced magnetic field. This has been proposed and used in the past [9, 31], and is formulated as follows. Split the magnetic field by

$$\boldsymbol{B} = \boldsymbol{B_0} + \boldsymbol{B_1}, \tag{82}$$

where

$$\frac{\partial \boldsymbol{B_0}}{\partial t} = 0;\ \nabla \cdot \boldsymbol{B_0} = 0;\ \nabla \times \boldsymbol{B_0} = 0. \tag{83}$$

The general fomulation becomes

$$\frac{\partial y_1}{\partial t} + \nabla \cdot \mathcal{F}(y_1, \nabla y_1) + \nabla \cdot \mathcal{G} - \mathcal{S}(y, \nabla y) = 0, \tag{84}$$

where

$$\mathcal{G} = \begin{pmatrix} 0 \\ (\boldsymbol{B_0} \cdot \boldsymbol{B_1})\mathcal{I} - (\boldsymbol{B_0 B_1} + \boldsymbol{B_1 B} - \boldsymbol{0}) \\ (\boldsymbol{B_0} \cdot \boldsymbol{B_1})\boldsymbol{v} - (\boldsymbol{v} \cdot \boldsymbol{B_1})\boldsymbol{B_0} \\ \boldsymbol{v B_0} - \boldsymbol{B_0 v} \end{pmatrix}. \tag{85}$$

So the existing resistive MHD solver, divergence cleaning and all, can be used in the flux calculations and numerical integration of the induced magnetic field $\boldsymbol{B_1}$, while the applied magnetic field $\boldsymbol{B_0}$ appears only in an additional flux term that is integrated separately.

Implementation of this formulation, with existing capabilities presented in this work, would provide an intuitive framework to model systems ranging from a magnetized plasma in a laboratory wind tunnel, to the interaction of the solar wind with the ionosphere. Thus, the modeling of constant, applied magnetic fields in an electrically conducting fluid is the next step that should be taken in the development of a plasma-dynamics solver for the study of electromagnetic interaction with hypersonic flows.

6. CONCLUSIONS

In this paper we motivated the development of a coupled electromagnetic-fluid dynamic solver for the multidisciplinary field of hypersonics, and presented the extension of a previously-reported MHD solver to include diffusive affects. We outlined the existing numerical model and solvers present in NRL's JENRE® Multiphysics Framework, and described the MHD capabilities that have been developed. The natural extension of the previously-developed ideal MHD solver was a resistive MHD solver, which accurately captures diffusion-dominated magnetic field affects while coupling the Navier-Stokes equations with Maxwell's electromagnetic equations.

We presented the fomulation of the resistive MHD equations in the context of a discontinuos Galerkin method, highlighted the important elements of the underlying MHD solver and the complexities involved with the addition of diffusive fluxes, and we have shown through multiple benchmarks the validity of our

resistive MHD implementation. These benchmarks increased progressively in complexity, demonstrating the clear effect of plasma conductivity on such important MHD concepts as magnetic reconnection and boundary layer formation.

Lastly, we have suggested a plan of action going forward, which aims to intuitively model external, applied magnetic fields separately from the weaker induced magnetic field in diffusion-dominated flows. The implementation of this capability should be followed by an evaluation of its efficacy in modeling the hypersonic systems that we are interested in. A multiple-temperature or multiple-species model may need to be pursued for certain specific plasma applications, such as plasma-assisted combustion. Regardless, the essential tools for MHD and plasma modeling in complex geometries are at the disposal of the Naval Research Laboratory and will be undergoing future development to be used extensively going forward.

ACKNOWLEDGMENTS

This work was made possible through the Karle's Fellowship Program at the U.S. Naval Research Laboratory.

REFERENCES

1. K. M. Hanquist, H. Alkandry, and I. D. Boyd, "Evaluation of computational modeling of electron transpiration cooling at high enthalpies," *Journal of Thermophysics and Heat Transfer* **31**(2), 283–293 (2017).

2. M. Kundrapu, J. Loverich, K. Beckwith, P. Stoltz, A. Shashurin, and M. Keidar, "Modeling radio communication blackout and blackout mitigation in hypersonic vehicles," *Journal of Spacecraft and Rockets* **52**(3), 853–862 (2015).

3. Y. X. Sha, H. L. Zhang, X. Y. Guo, and M. Y. Xia, "Analyses of electromagnetic properties of a hypersonic object with plasma sheath," *IEEE Transactions on Antennas and Propagation* **67**(4), 2470–2481 (2019).

4. R. L. Kimmel, D. Adamczak, D. Hartley, H. Alesi, M. A. Frost, R. Pietsch, J. Shannon, and T. Silvester, "HIFiRE-5b flight overview," Proceedings of the 47th AIAA Fluid Dynamics Conference, 2017, p. 3131.

5. W. L. Jones and A. E. Cross, *Electrostatic-probe measurements of plasma parameters for two reentry flight experiments at 25000 feet per second*, volume 6617 (National Aeronautics and Space Administration, 1972).

6. P. Mocz, M. Vogelsberger, D. Sijacki, R. Pakmor, and L. Hernquist, "A discontinuous Galerkin method for solving the fluid and magnetohydrodynamic equations in astrophysical simulations," *Monthly Notices of the Royal Astronomical Society* **437**(1), 397–414 (2014).

7. C. L. Bachman and A. Kercher, "A Discontinuous Galerkin Method for Ideal Magnetohydrodynamics in NRL's JENRE® Code," *Defense Technical Information Center* (2022).

8. A. Dedner, F. Kemm, D. Kröner, C. D. Munz, T. Schnitzer, and M. Wesenberg, "Hyperbolic divergence cleaning for the MHD equations," *Journal of Computational Physics* **175**(2), 645–673 (2002).

9. K. G. Powell, P. L. Roe, T. J. Linde, T. I. Gombosi, and D. L. De Zeeuw, "A solution-adaptive upwind scheme for ideal magnetohydrodynamics," *Journal of Computational Physics* **154**(2), 284–309 (1999).

10. R. Hartmann and T. Leicht, "Higher order and adaptive DG methods for compressible flows," in H. Deconinck, ed., *VKI LS 2014-03: 37th Advanced VKI CFD Lecture Series: Recent developments in higher order methods and industrial application in aeronautics, Dec. 9-12, 2013* (Von Karman Institute for Fluid Dynamics, Rhode Saint Genèse, Belgium, 2014). Retrieved from `https://ganymed.math.uni-heidelberg.de/~hartmann/publications/2014/HL14a.pdf`.

11. A. Corrigan, D. Williams, and A. Kercher, "Weak formulation of a conservation law in reference space," 2020.

12. P. Cargo and G. Gallice, "Roe matrices for ideal MHD and systematic construction of Roe matrices for systems of conservation laws," *Journal of Computational Physics* **136**(2), 446–466 (1997).

13. J. M. Stone, T. A. Gardiner, P. Teuben, J. F. Hawley, and J. B. Simon, "Athena: a new code for astrophysical MHD," *The Astrophysical Journal Supplement Series* **178**(1), 137 (2008).

14. F. Bassi and S. Rebay, "An implicit high-order discontinuous Galerkin method for the steady state compressible Navier-Stokes equations," *Computational fluid dynamics'98* pp. 1226–1233 (1998).

15. F. Bassi and S. Rebay, "GMRES discontinuous Galerkin solution of the compressible Navier-Stokes equations," in *Discontinuous Galerkin Methods*, pp. 197–208 (Springer, 2000).

16. F. Bassi and S. Rebay, "Numerical evaluation of two discontinuous Galerkin methods for the compressible Navier–Stokes equations," *International journal for numerical methods in fluids* **40**(1-2), 197–207 (2002).

17. H. L. Atkins and C. W. Shu, "Quadrature-free implementation of discontinuous Galerkin method for hyperbolic equations," *AIAA journal* **36**(5), 775–782 (1998).

18. D. Derigs, A. R. Winters, G. J. Gassner, S. Walch, and M. Bohm, "Ideal GLM-MHD: About the entropy consistent nine-wave magnetic field divergence diminishing ideal magnetohydrodynamics equations," *Journal of Computational Physics* **364**, 420–467 (2018).

19. F. Bassi, F. Cecchi, N. Franchina, S. Rebay, and M. Savini, "High-order discontinuous Galerkin computation of axisymmetric transonic flows in safety relief valves," *Computers & fluids* **49**(1), 203–213 (2011).

20. R. Hartmann and T. Leicht, "Higher order and adaptive DG methods for compressible flows," *37th Advanced CFD Lecture Series: Recent developments in higher order methods and industrial application in aeronautics* **2014**(3), 1–156 (2014).

21. R. F. Johnson and A. D. Kercher, "A conservative discontinuous Galerkin discretization for the chemically reacting Navier-Stokes equations," *Journal of Computational Physics* **423**, 109826 (2020).

22. A. J. Wright and I. Hawke, "A resistive extension for ideal magnetohydrodynamics," *Monthly Notices of the Royal Astronomical Society* **491**(4), 5510–5523 (2020).

23. A. Mignone, C. Zanni, P. Tzeferacos, B. Van Straalen, P. Colella, and G. Bodo, "The PLUTO code for adaptive mesh computations in astrophysical fluid dynamics," *The Astrophysical Journal Supplement Series* **198**(1), 7 (2011).

24. P. Sweet, "14. The neutral point theory of solar flares," Proceedings of the Symposium-International Astronomical Union, volume 6 (Cambridge University Press), 1958, pp. 123–134.

25. E. N. Parker, "Sweet's mechanism for merging magnetic fields in conducting fluids," *Journal of Geophysical Research* **62**(4), 509–520 (1957).

26. D. Biskamp, "Magnetic reconnection via current sheets," *The Physics of fluids* **29**(5), 1520–1531 (1986).

27. R. J. Moreau, *Magnetohydrodynamics*, volume 3 (Springer Science & Business Media, 1990).

28. N. Ben Salah, A. Soulaimani, W. G. Habashi, and M. Fortin, "A conservative stabilized finite element method for the magneto-hydrodynamic equations," *International Journal for Numerical Methods in Fluids* **29**(5), 535–554 (1999).

29. J. N. Shadid, R. P. Pawlowski, J. W. Banks, L. Chacón, P. T. Lin, and R. S. Tuminaro, "Towards a scalable fully-implicit fully-coupled resistive MHD formulation with stabilized FE methods," *Journal of Computational Physics* **229**(20), 7649–7671 (2010).

30. R. J. Moreau, *Magnetohydrodynamics*, volume 3 (Springer Science & Business Media, 1990).

31. T. Tanaka, "Finite volume TVD scheme on an unstructured grid system for three-dimensional MHD simulation of inhomogeneous systems including strong background potential fields," *Journal of Computational Physics* **111**(2), 381–389 (1994).